

Understanding the Limits of Plasmonic Enhancement in Organic Photovoltaics

William R. Erwin,[†] Roderick C. I. MacKenzie,^{‡*} Rizia Bardhan^{†*}

[†]Department of Chemical and Biomolecular Engineering, Vanderbilt University, Nashville, Tennessee, 37235, United States. [‡]Faculty of Engineering, University of Nottingham, Nottingham, Nottinghamshire, NG7 2RD, UK

*E-mail: rizia.bardhan@vanderbilt.edu; roderick.mackenzie@nottingham.ac.uk

ABSTRACT

Plasmonic enhancement in organic photovoltaics (OPVs) has been extensively studied in the past decade. However, the improvements in power conversion efficiency (PCE) is highly inconsistent in literature findings due to poor understanding of the limitations of plasmonic approach in OPVs. In this work, we address these long-standing uncharted questions with a model system consisting of PCPDTBT:PC₆₁BM polymer active layer with silver nanostructures embedded in the PEDOT: PSS hole transport layer. Our study demonstrates that (i) plasmonic enhancement is highly shape-dependent where Ag nanosphere incorporated OPVs show higher PCE than Ag nanocubes, (ii) plasmonic enhancement is strongly localized within the hole transport layer where PCE is primarily enhanced due to an increase in the exciton generation and carrier collection efficiency, (iii) unlike common belief light absorption efficiency in the active layer has minimal impact on PCE due to the detrimental light blocking effect of metal nanostructures, and (iv) plasmonic enhancements are most pronounced when the charge carrier mobility of the electron donor and electron acceptor materials are unbalanced but results in losses in OPVs with balanced charge transport. The findings of our work provides a generalized framework to guide researchers on the parameters that can be systematically optimized to maximize plasmonic enhancement in OPVs as well as other solar devices.

INTRODUCTION

Organic photovoltaics (OPVs) are an exciting solar technology due to their low cost of solution processing, and amenability to large scale production enabled by their lightweight, small footprint, and flexible architectures.¹⁻³ Nonetheless, power conversion efficiency (PCE) of OPVs remain modest relative to other classes of emerging PVs such as perovskite solar cells attributable to both limited spectral absorption and poor charge transport.⁴⁻⁶ The bulk heterojunction (BHJ) architecture of OPVs is most effective for achieving high performance due to the bicontinuous interpenetrating network between the donor the acceptor molecules in the active layers driving exciton dissociation and carrier transport.⁷⁻⁹ However the active layer thicknesses in BHJ OPVs is limited to ~150 nm to facilitate charge transport which inherently limits the total light harvested in the layer. In the past decade, the integration of plasmonic nanostructures both in the active layer and the hole transport layer (HTL) has demonstrated tremendous improvements in OPVs.¹⁰⁻¹³ This has been primarily correlated to improved light harvesting via radiative enhancement mechanisms which include light scattering and concentrated local electromagnetic fields.^{3, 10, 14} A few studies have also attributed plasmonic enhancement to hot carrier injection,¹⁵ and coupling of plasmons with excitons in the organic semiconductors.¹⁶⁻¹⁷ In our recent work we showed increased light absorption and enhanced carrier generation in OPVs when shape-controlled metal nanostructures were positioned at the interface of the active layer and HTL.¹⁸ These carriers localized at the interface allowed shorter carrier diffusion length and rapid carrier collection in the plasmon enhanced OPVs. Whereas a range of morphological- and compositional-tunable metal nanostructures have been employed in OPVs,^{11, 19-20} the improvements in PCE reported¹¹ in the literature are often inconsistent from one study to another. This is attributed to the lack of our understanding of the limitations of

plasmonic approach which includes the regimes where metallic nanostructures are ineffective or result in losses in OPVs. Further, the properties of the organic polymers, specifically the charge mobilities, also play a role towards overall enhancements in presence of metal nanostructures.

In this work, we address these uncharted questions by investigating the optical and electronic effects of OPVs consisting of PCPDTBT:PC₆₁BM (poly[2,6-(4,4-bis-(2-ethylhexyl)-4H-cyclopenta[2,1-b;3,4-b']dithiophene)-alt-4,7-(2,1,3-benzothiadiazole)]:[6,6]-phenyl C₆₁ butyric acid methyl ester) active layer with either silver nanospheres (AgNS) or silver nanocubes (AgNC) integrated into the PEDOT:PSS (poly(3,4-ethylenedioxythiophene): polystyrene sulfonate) HTL. Plasmonic enhancement of PCPDTBT:PCBM based OPVs has shown improvement in PCE of devices and has been correlated to enhanced light capture in the visible (450-650 nm) where PCPDTBT has poor light absorption.^{3, 21} The objective of our computational study is to use this model OPV system and establish a mechanistic understanding that will guide experimentalists on the parameters that can be carefully optimized to achieve plasmon enhanced OPVs and examine the regimes where metal nanostructures will be detrimental to device performance. Here, we first studied how the shape of the Ag nanostructure and the corresponding optical properties contribute to absorption enhancements. And second we also studied how the carrier mobilities of PCPDTBT:PCBM active layer directly impact the efficiencies of plasmonic OPVs.^{10, 22-25} To demonstrate the impact of both optical and electronic effects that arise in the presence of metal nanostructures, we combined two simulation regimes. We first solved for the optical enhancements via plasmonic effects using finite difference time domain (FDTD) electromagnetic simulations which numerically solves Maxwell's Equations to examine absorption profiles of the photovoltaic material. We then used these electrodynamic simulations to solve for the electrical behavior of the solar cell using the general-purpose

photovoltaic device model (GPVDM) which solves both electron and hole drift-diffusion equations in position space to describe the movement of charge within a device. The GPVDM allows the carrier population to be resolved in both position and energy space which allows us to examine recombination with balanced or unbalanced charge carriers.

Whereas we chose to study a model OPV system here, this work provides simple design rules that can be generalized to understand plasmonic enhancement in other polymer solar cells, and broadly in a number of emerging thin-film PVs such as planar perovskite solar cells and tandem solar cells. This is leveraged by the use of both FDTD and GPVDM models which have successfully characterized optical and electronic behavior in a range of organic and semiconductor devices.²⁶⁻²⁸ Further the carrier population characteristics investigated here can be applied to other classes of optoelectronic devices such as photodetectors, field effect transistors, and sensors where plasmonic nanostructures have improved detection limits.²⁹⁻³² We anticipate this work will allow researchers to manipulate and modulate various factors, such as the choice of the semiconductor material and the plasmonic nanostructure morphology, to achieve the maximum possible PCE in OPVs and other optoelectronic devices.

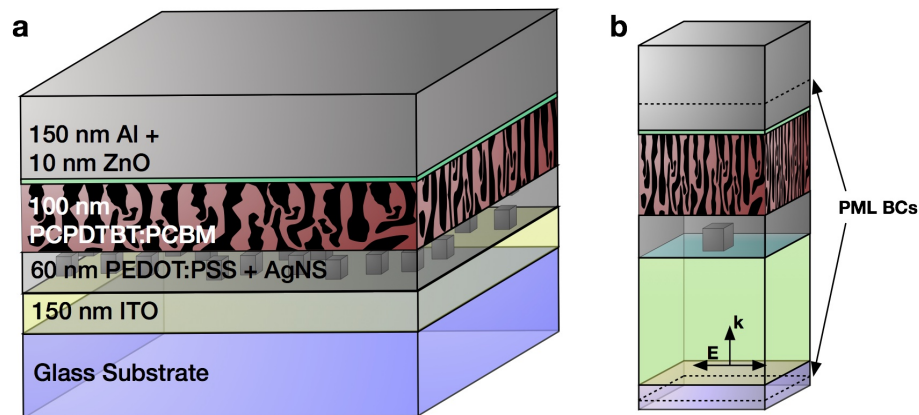


Figure 1: (a) Schematic of plasmon enhanced organic photovoltaics with Ag nanostructures incorporated in the PEDOT:PSS hole transport layer. (b) Simulation schematic of device where perfectly matched layer (PML) boundary conditions (BC) are used in the z-dimension to simulate an unbounded medium, and periodic BCs are used in the x and y dimensions.

RESULTS AND DISCUSSION

In this study, we incorporated 50 nm diameter Ag nanospheres (AgNS) and 50 nm edge length nanocubes (AgNC) in the PEDOT:PSS layer of OPVs with PCPDTBT:PCBM active layer accompanied with a thin ZnO electron transport later and Al charge collector (Fig. 1a). The device structure consists of 150 nm ITO/60 nm PEDOT:PSS/100 nm PCPDTBT:PCBM/10 nm ZnO/100 nm Al, which was chosen to match experimental device architecture reported in the literature.^{10, 33} The simulation schematic is shown in figure 1b and a detailed description of the simulation methods is provided in the Methods section. The utility of Ag nanostructures are ideal for light harvesting in OPVs due to the low optical losses of Ag in the visible, the ease of colloidal synthesis resulting in shape and size- controlled nanostructures, and Ag plasmon resonance compliments the absorbance of PCPDTBT enabling broadband light absorption (Figure 2). By comparing two different Ag nanostructure morphologies, we studied the contributions of the absorption and scattering properties of each geometry (Fig. 2a) towards the performance of the OPVs. Note that the scattering cross section of both AgNS and AgNC spectrally overlaps with the region of poor absorption of PCPDTBT (Fig. 2b) and serves to enhance the carrier generation in the active layer of the OPVs specifically in the vicinity of the nanostructure. The different morphologies also controls the ratio of light scattered to light absorbed. Whereas AgNC have 1:1 ratio of scattering to absorption, AgNS have ~3:1 ratio; the contribution of scattering to absorption directly governs the light absorbed in the device. In addition to light harvesting, the exciton generation efficiency as well as the charge collection efficiency are equally important towards overall PCE. This can be understood by examining the equation for the wavelength dependent external quantum efficiency (EQE) given by:

$$EQE(\lambda) = \eta_{\text{scat}} \times \eta_{\text{gen}} \times \eta_{\text{coll}} \quad (1)$$

where η_{abs} is the ratio of absorbed light to incident light, η_{gen} is the ratio of photoexcited excitons that are converted to free carriers, and η_{coll} is the ratio of the generated free carriers that reach the electrode prior to recombination, and are collected after the final interface between the active layer and the electrodes.^{3, 34-35}

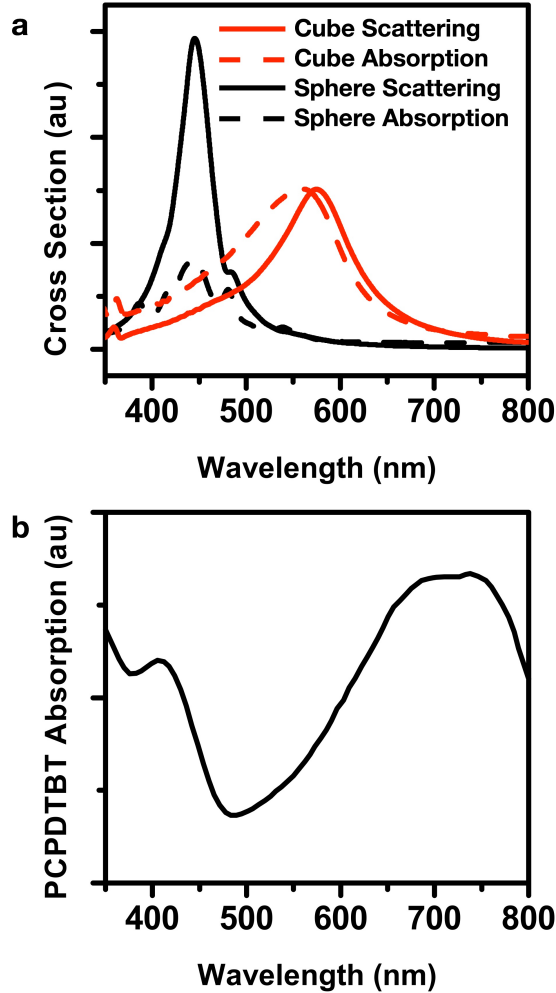


Figure 2. a) Absorption and scattering profiles of 50 nm diameter AgNS and 50 nm edge length AgNC which overlap with the low absorption area of the PCPDTBT polymer system. b) The absorption spectrum of the active layer polymer PCPDTBT.

Therefore, to understand the impact of AgNS and AgNC on η_{abs} , η_{gen} and η_{coll} , we

conducted FDTD optical simulations of reference and nanostructure embedded PCDPTBT:PCBM OPVs. Optical coefficients for the polymers and charge transport layers were adapted from the literature.^{21, 36-37} We calculated the power absorbed (P_{abs}) by the active layer using both AgNCs and AgNSs given by the equation,

$$P_{|\omega|=\omega} = \int E^2 \epsilon_2 \, dV \quad (2)$$

where ω is the frequency, E is the electric field calculated via FDTD, and ϵ_2 is the imaginary part of the dielectric constant of the polymer active layer. We examined the fraction of light absorbed by the active layer as a function of wavelength for the reference and plasmon enhanced devices (Fig. 3a). Our calculations show that the improvement in absorption via light harvesting by the Ag nanostructures is both shape-dependent and wavelength-dependent. The fraction of light absorbed in the active layer improves for the AgNS in the 450-600 nm range where only a small amount of light is being absorbed by the AgNS and significant amount of light is scattered and harvested by the active layer. The AgNS gives rise to a 4.6% improvement in light absorbed in the visible (Fig.3a) relative to the reference device when integrated over the AM 1.5G solar spectrum. Whereas we expected that AgNC would result in a larger enhancement in light absorption given the strong local electric fields in the edges and corners of AgNC, to our surprise AgNC compromises light harvesting in the active layer by 16.6% throughout the visible region. This is attributable to the high absorption cross section of AgNC relative to scattering implying that incident photons are absorbed by the metal before reaching the active layer.

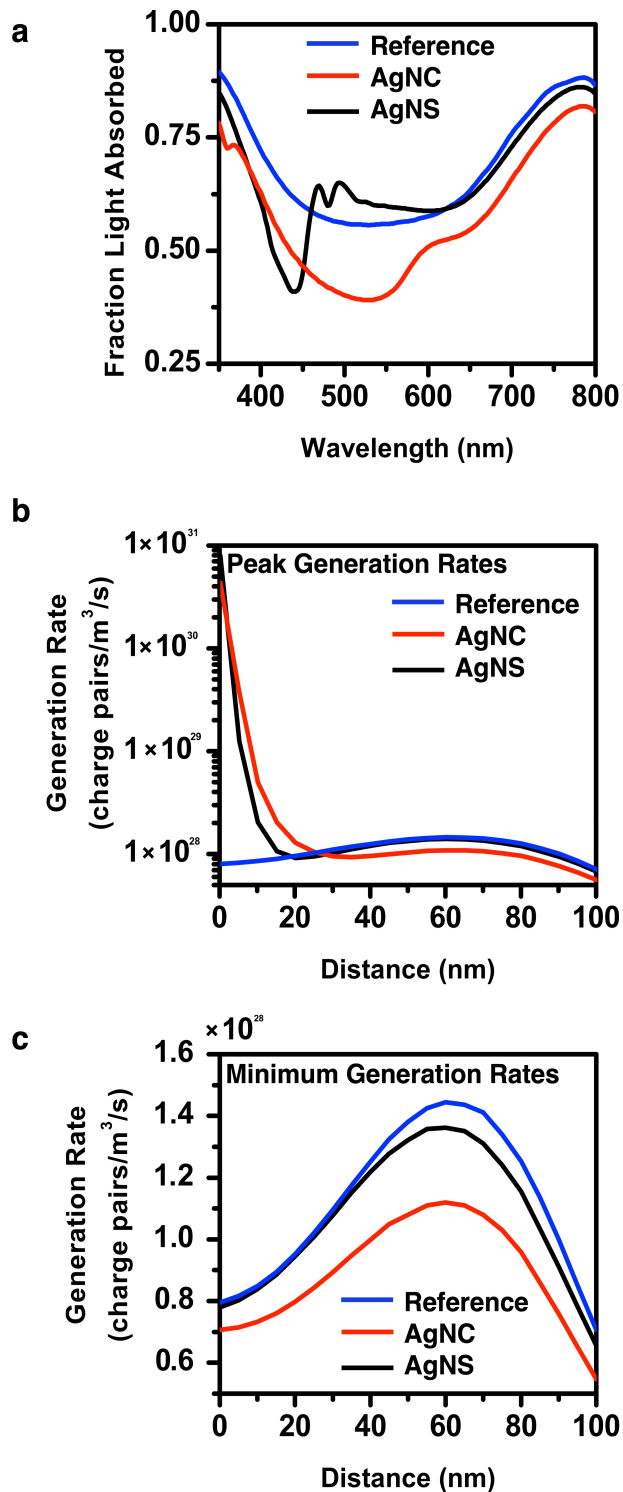


Figure 3: (a) The fraction of incident light that is absorbed as a function of wavelength for the reference and plasmon enhanced devices. Spatially varying exciton generation rate at the (b) maximum and (c) minimum for devices incorporating AgNS and AgNC. The x-axis represents the location in the active layer where 0 being close to the hole transport layer and 100 being close to the electron transport layer.

Whereas it is counter-intuitive that an overall reduction in η_{abs} through the active layer can result in improved device performance, the high electric field concentrations surrounding the metal nanostructures enhance η_{gen} and η_{coll} as shown in figure 3b-c. The incorporation of plasmonic nanostructures into the HTL of an OPV creates a distortion of the active layer in three dimensions i.e. light absorption rate is not homogeneous in the planar dimension. This nonhomogeneous absorption rate gives rise to spatially variable exciton generation rate which peaks near the nanostructure surface where local field effects are strongest. In order to investigate the effect of field concentration on the performance of our OPV system near the interface of active layer/HTL, we considered the photon absorption in discrete spatial regions. Using the assumption that each absorbed photon translated to a single exciton, we calculated the generation rate by dividing the power absorbed (P_{abs}) by the energy per photon and integrating over the AM 1.5G solar spectrum. The resulting carrier generation rates in figure 3b-c are given as a function of the depth of the active layer where 0 nm corresponds to the bottom of the active layer near the HTL, and 100 nm corresponds to the top of the active layer far from the embedded nanostructures. The maximum generation rates (Fig. 3b) are localized within 25 nm distance near the HTL where the nanostructures are embedded, and are clearly shape-dependent. Due to the intense electric fields localized at the edges and corners of AgNC, η_{gen} is high within the electric field decay length, but beyond 25 nm AgNCs have a detrimental effect. AgNS also improve generate rate within ~ 20 nm and have minimal impact on the overall device performance beyond that. The minimum generation rates (Fig. 3c) indicates that away from the HTL/active layer interface, the presence of the nanostructures decreases exciton generation through the bulk of the active layer when compared to the reference device.

To further understand the localized effect of the plasmonic nanostructures, we examined the spatially dependent electric field enhancement in the devices at a wavelength of 500 nm using FDTD simulations (Figure 4). The cross sections of the active layer where the electric field is normalized to the reference device bisecting the nanostructures is shown in Figure 4a-b. The AgNS and AgNC are in the HTL and the active layer is discretized into three sections labeled “close,” “mid,” and “far,” in reference to their distance from the nanostructures. The E-field profiles show that both nanostructures have forward scattering into the active layer, which is more pronounced for the AgNS relative to AgNC. Further, the spatially dependent average electric field intensity of the nanostructures is up to 20× the incident field but localized within 20 nm of the active layer/HTL interface. Next we calculated the absorption enhancement in the active layer (Figure 4c-d) for the plasmon enhanced devices normalized to the reference device for the spatial sections of the active layer. Whereas AgNS significantly improves the absorption in the region of the active layer closest to the HTL, farther away from the HTL interface the presence of AgNS has detrimental effect on light absorbed by the active layer. The AgNC results in overall decreased absorption (absorption enhancement < 1) for all spatial sections of the active layer since much of the light is absorbed by the AgNC with minimal light scattered into the active layer.

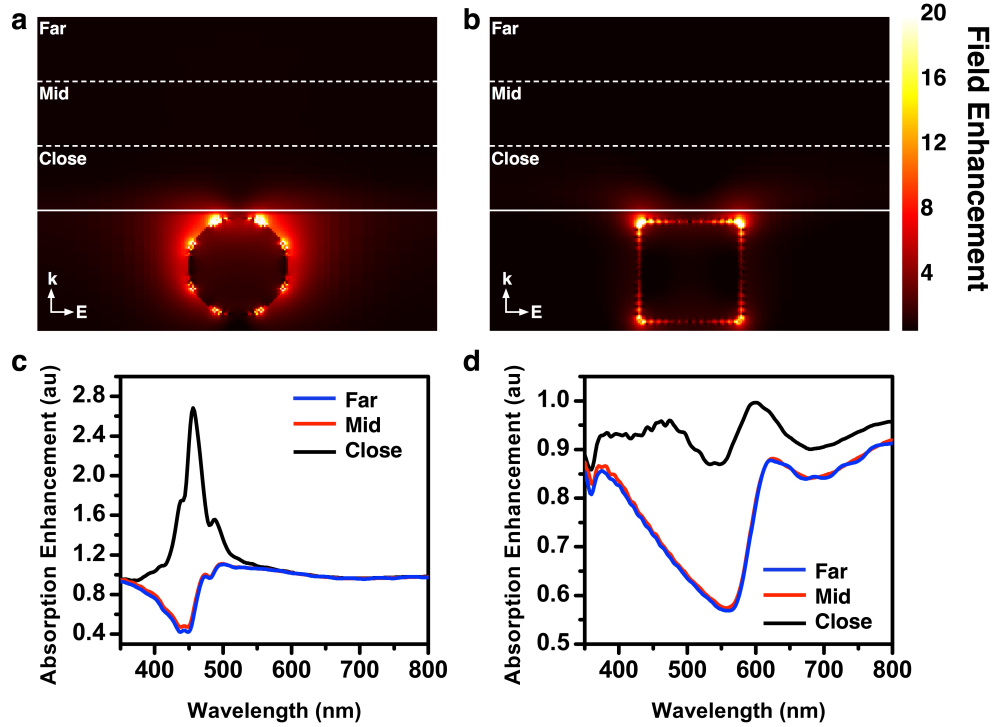


Figure 4: Field profiles in the hole transfer layer and active layer for devices containing a) AgNS and b) AgNC normalized to the reference device at $\lambda = 500$ nm. The corresponding absorption enhancement normalized to the reference device for the spatial sections of the active layer illustrated in (a) – (b) for devices with c) AgNS and d) AgNC.

Next, to understand the effect of η_{abs} and η_{gen} in the active layer and how that impacts the device efficiencies of OPVs, we performed electrical simulations and calculated the spatially variant PCE through the active layer normalized to the reference device with GPVDM.³⁸⁻³⁹ We simulated two scenarios: PCDPTBT:PCBM OPV with balanced charge carriers (hole mobility = electron mobility) and an OPV with unbalanced charge carrier that is “hole-limited” (hole mobility \ll electron mobility).^{21, 24, 40-41} When a generation rate profile is input into GPVDM, the model uses the finite difference method to solve electron and hole drift diffusion equations as well as the carrier continuity equations to describe the movement of charges in the device in one dimension. Recombination is taken into account by Langevin (free carrier) recombination, as well as Shockley-Read-Hall (free-to-trap) recombination.⁴²⁻⁴³ The

overall current-potential scans for the balanced and unbalanced charge mobilities (Fig. 5a,b) shows that hole-limited reference OPVs perform poorly (2.60%) relative to those with balanced carriers (4.83%). Interestingly, a significant improvement in PCE is observed when the plasmonic nanostructures are integrated in hole-limited OPVs resulting in 9.9% increase in PCE with AgNS and 9.1% increase with AgNC. However, devices with balanced charge carriers show minimal improvements in PCE with plasmonic nanostructures. AgNS resulted in a 2.9% increase in PCE whereas AgNC decreased the PCE by -7.9% relative to reference OPVs. The drop in PCE calculated in the AgNC device is correlated to the drastic decrease in exciton generation rate in the bulk of the active layer (see Figure 3c). We also simulated a spatial map of the PCE in the vicinity of the nanostructures (Fig. 5c-f) which show the localization of high PCE overlaps with the areas of strong electric field concentration and reflects the trends observed in the J-V curves. Note that the spatial profile shown for AgNS is a nanosphere viewed from the top with near-field enhancements concentrated within a localized area.

Overall this study provides a simplistic overview of how the choice of the metal nanostructure employed and the properties of the active material can considerably impact the observed increase or decrease in solar cell performance. First we observe that plasmonic enhancement is shape-dependent, and whereas non-spherical geometries have shown higher enhancements in OPVs, our simulations show the stronger scattering cross-section of AgNS compliments the spectral region where PCPDTBT:PCBM poorly absorbs and improves fraction of light absorbed in the active layer relative to AgNC. Second our simulations show the detrimental light blocking effect of metal nanostructures diminishes the overall η_{abs} in the active layer where the presence of AgNS and AgNC decreases the overall absorption by 2.3% and 16.6% respectively. Third our electric field profiles shows that the intense light concentration

near the HTL/active layer interface where the plasmonic nanostructures are localized improves η_{gen} and η_{coll} since majority of the excitons in the plasmon enhanced OPVs now have a short carrier diffusion length enabling carrier to be collected before the detrimental effect of charge trapping in BHJ OPVs.⁴⁴⁻⁴⁵ And fourth, plasmonic enhancement is most effective in OPVs where the polymer system has unbalanced charge carriers such as hole-limited or electron-limited (not shown here). During experiments, unbalanced carriers may arise from human errors during the fabrication and processing techniques, or use of low molecular weight polymers which can result in poor-performing reference OPVs. OPVs with balanced carrier mobilities will have minimal impact or even undesirable losses from plasmonic nanostructures.

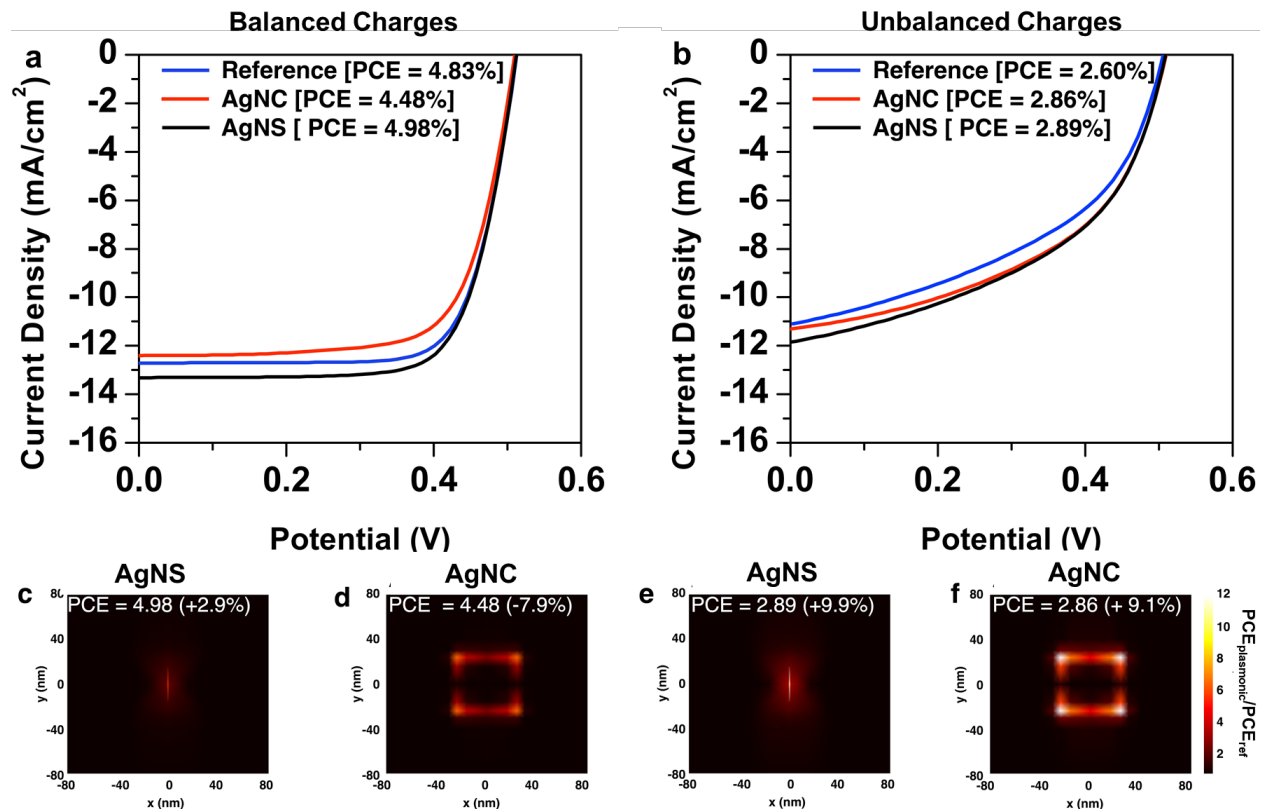


Figure 5. Current-Voltage scans of reference and plasmonic devices with polymer systems that have a) balanced carrier mobilities and b) unbalanced charge carriers with a hole carrier minority. Power conversion efficiency map normalized to the reference PCE for balanced carriers with c) AgNS, and d) AgNC, and for hole minority carrier with e) AgNS and f) AgNC.

CONCLUSIONS

In summary, in this work we show that improved power conversion efficiency of plasmon-enhanced organic photovoltaics is strongly dependent on the metal nanostructure geometry and the resulting scattering cross-section. Further, we emphasize that when plasmonic nanostructures are embedded in the hole transport layer, the observed optical enhancement may not necessarily result from improved light capture in the active layer, but rather comes from field intensity modulation near the interface of active layer/hole transport layer. In addition, incorporation of plasmonic nanostructures is effectively only useful in OPVs with unbalanced charge carrier mobility, for example when hole mobility \ll electron mobility, a phenomenon that has not been previously understood in the literature. Our study provides simple design rules that researchers can straightforwardly apply to fabricate plasmonic OPVs by designing metal nanostructures with strong forward scattering optimized for the spectral regions where the active layer organic polymer poorly absorbs, and understand the regimes where metal nanostructures will be ineffective or will result in losses. Our simulation approach can ultimately be scaled to enable broad screening of polymers and nanostructure geometries for efficient device design. This work can also be extended to plasmonic enhancement in a range of thin-film and mesoporous solar cells,⁴⁶⁻⁴⁸ as well as other solar energy conversion devices,⁴⁹⁻⁵⁰ and localized plasmon resonance sensors.⁵¹

SIMULATION METHODS

Optical Simulations: Absorption and scattering are calculated in Lumerical FDTD solutions using the total-field scattered-field (TFSF) incident light source. The function of the TFSF source

is to inject a source frequency (in this case a pulse spanning the 350-800 nm frequency range) into a specific simulation volume where it interacts with a nanostructure. The injected incident field is then removed outside the TFSF boundaries, allowing a simple energy balance to measure the absorption and scattering cross sections. Periodic boundary conditions are used in the lateral direction, as they provide a feasible route to realistic large scale simulations of thin film PVs. It has been shown in other thin film systems that periodic results approximate the real world system where more disorder is often present.⁵²⁻⁵³ Perfectly matched layer (PML) absorbing boundary conditions are used in the z-dimension to simulate dissipation into free space (i.e. to avoid internal reflections which introduce error into the simulation). Upon simulation convergence, the electric field concentration in the active layer is recorded - this can be used to compute the spatially variant generation rate which can then be imported into an electrical solver to simulate solar cell performance under real world conditions.

Electrical Simulations: Electrical simulations were carried out using the General Purpose Photovoltaic Device Model (GPVDM).³⁹ GPVDM uses a finite difference approach to solve both electron and hole drift-diffusion equations to describe the movement of charge within the device. At each mesh point in position space, a set of carrier trapping and escape equations are solved in energy space where excitonic recombination can occur via a free-to-free Langevin type recombination or by free-to-trap Shockley-Read-Hall type recombination. Therefore, GPVDM allows the carrier population to be resolved in both position and energy space. Generation rates from FDTD optical simulation were imported directly into GPVDM. For balanced devices, the electron and hole mobility were set to $1 \times 10^{-5} \text{ m}^2\text{V}^{-1}\text{s}^{-1}$, and for the unbalanced devices the electron and hole mobilities were set to $1 \times 10^{-5} \text{ m}^2\text{V}^{-1}\text{s}^{-1}$ and $1 \times 10^{-8} \text{ m}^2\text{V}^{-1}\text{s}^{-1}$, respectively. For plasmonics devices, individual simulations were conducted for different carrier generation rates

associated with various spatial positioning, the results were spatially averaged to compute the electrical properties.

ACKNOWLEDGEMENTS

WRE acknowledges support from the National Science Foundation Graduate Research Fellowship Program under Grant Number 1445197.

REFERENCES

1. Ameri, T.; Dennler, G.; Lungenschmied, C.; Brabec, C. J., Organic Tandem Solar Cells: A Review. *Energ. Environ. Sci.* **2009**, *2*, 347-363.
2. Ameri, T.; Khoram, P.; Min, J.; Brabec, C. J., Organic Ternary Solar Cells: A Review. *Adv. Mater.* **2013**, *25*, 4245-4266.
3. Chou, C.-H.; Chen, F.-C., Plasmonic Nanostructures for Light Trapping in Organic Photovoltaic Devices. *Nanoscale* **2014**, *6*, 8444-8458.
4. Chen, D.; Nakahara, A.; Wei, D.; Nordlund, D.; Russell, T. P., P3ht/Pcbm Bulk Heterojunction Organic Photovoltaics: Correlating Efficiency and Morphology. *Nano Lett.* **2011**, *11*, 561-567.
5. Lin, Y.; Li, Y.; Zhan, X., Small Molecule Semiconductors for High-Efficiency Organic Photovoltaics. *Chem. Soc. Rev.* **2012**, *41*, 4245-4272.
6. Zhang, S.; Ye, L.; Hou, J., Breaking the 10 % Efficiency Barrier in Organic Photovoltaics : Morphology and Device Optimization of Well-Known Pbdttt Polymers. *Adv. Energy Mater.* **2016**, *6*, 1502529-1502529.
7. Narayan, M. R.; Singh, J., Roles of Binding Energy and Diffusion Length of Singlet and Triplet Excitons in Organic Heterojunction Solar Cells. *Phys. Status Solidi a* **2012**, *9*, 2386-2389.
8. Scharber, M. C.; Mühlbacher, D.; Koppe, M.; Denk, P.; Waldauf, C.; Heeger, A. J.; Brabec, C. J., Design Rules for Donors in Bulk-Heterojunction Solar Cells - Towards 10 % Energy-Conversion Efficiency. *Adv. Mater.* **2006**, *18*, 789-794.
9. Dennler, B. G.; Scharber, M. C.; Brabec, C. J., Polymer-Fullerene Bulk-Heterojunction Solar Cells. *Adv. Mater.* **2009**, *21*, 1323-1338.
10. Baek, S. W.; Noh, J.; Lee, C. H.; Kim, B.; Seo, M. K.; Lee, J. Y., Plasmonic Forward Scattering Effect in Organic Solar Cells: A Powerful Optical Engineering Method. *Sci. Rep.* **2013**, *3*, 1-7.
11. Baek, S. W.; Park, G.; Noh, J.; Cho, C.; Lee, C. H.; Seo, M. K.; Song, H.; Lee, J. Y., Au@Ag Core-Shell Nanocubes for Efficient Plasmonic Light Scattering Effect in Low Bandgap Organic Solar Cells. *ACS Nano* **2014**, *8*, 3302-3312.
12. Gan, Q.; Bartoli, F. J.; Kafafi, Z. H., Plasmonic-Enhanced Organic Photovoltaics: Breaking the 10% Efficiency Barrier. *Adv. Mater.* **2013**, *25*, 2385-2396.

13. Wadams, R. C.; Yen, C.-w.; Butcher, D. P.; Koerner, H.; Durstock, M. F.; Fabris, L.; Tabor, C. E., Gold Nanorod Enhanced Organic Photovoltaics: The Importance of Morphology Effects. *Org. Electron.* **2014**, *15*, 1448-1457.
14. Yoon, W.-J.; Jung, K.-Y.; Liu, J.; Duraisamy, T.; Revur, R.; Teixeira, F. L.; Sengupta, S.; Berger, P. R., Plasmon-Enhanced Optical Absorption and Photocurrent in Organic Bulk Heterojunction Photovoltaic Devices Using Self-Assembled Layer of Silver Nanoparticles. *Solar Energ. Mater. and Solar Cells* **2010**, *94*, 128-132.
15. Wang, C.; Li, C.; Wen, S.; Ma, P.; Liu, Y.; Mackenzie, R. C. I., Combining Plasmonic Trap Filling and Optical Backscattering for Highly Efficient Third Generation Solar Cells. *J. Mater. Chem. A* **2017**, *5*, 3995-4002.
16. Chen, F. C.; Wu, J. L.; Lee, C. L.; Hong, Y.; Kuo, C. H.; Huang, M. H., Plasmonic-Enhanced Polymer Photovoltaic Devices Incorporating Solution-Processable Metal Nanoparticles. *Appl. Phys. Lett.* **2009**, *95*, 93-96.
17. Wu, J. L.; Chen, F. C.; Hsiao, Y. S.; Chien, F. C., Surface Plasmonic Effects of Metallic Nanoparticles on the Performance of Polymer Bulk Heterojunction Solar Cells. *ACS Nano* **2011**, *5*, 959-967.
18. Erwin, W. R.; Hungerford, C.; Zarick, H. F.; Talbert, E. M.; Arora, P.; Bardhan, R., Enhancement in Organic Photovoltaics Controlled by the Interplay between Charge-Transfer Excitons and Surface Plasmons. *ACS Omega* **2016**, *1*, 722-729.
19. Fung, D. D. S.; Qiao, L.; Choy, W. C. H.; Wang, C.; Sha, W. E. I.; Xie, F.; He, S., Optical and Electrical Properties of Efficiency Enhanced Polymer Solar Cells with Au Nanoparticles in a Pcdot-Pss Layer. *J. Mater. Chem* **2011**, *21*, 16349-16349.
20. Li, X., et al., Dual Plasmonic Nanostructures for High Performance Inverted Organic Solar Cells. *Adv. Mater.* **2012**, *24*, 3046-52.
21. Albrecht, S.; Schäfer, S.; Lange, I.; Yilmaz, S.; Dumsch, I.; Allard, S.; Scherf, U.; Hertwig, A.; Neher, D., Light Management in Pcpdtbt:PC70BM Solar Cells: A Comparison of Standard and Inverted Device Structures. *Org. Electron.* **2012**, *13*, 615-622.
22. Arinze, E. S.; Qiu, B.; Nyirjesy, G.; Thon, S. M., Plasmonic Nanoparticle Enhancement of Solution-Processed Solar Cells: Practical Limits and Opportunities. *ACS Photonics* **2016**, *3*, 158-173.
23. Haidari, G.; Hajimahmoodzadeh, M.; Fallah, H. R.; Peukert, A.; Chanaewa, A.; Hauff, E. V., Thermally Evaporated Ag Nanoparticle Films for Plasmonic Enhancement in Organic Solar Cells : Effects of Particle Geometry. *Phys. Status Solidi* **2015**, *165*, 161-165.
24. Wang, D. H.; Kim, D. Y.; Choi, K. W.; Seo, J. H.; Im, S. H.; Park, J. H.; Park, O. O.; Heeger, A. J., Enhancement of Donor-Acceptor Polymer Bulk Heterojunction Solar Cell Power Conversion Efficiencies by Addition of Au Nanoparticles. *Angew. Chem.* **2011**, *123*, 5633-5637.
25. Xu, X.; Ko, A.; Kyaw, K.; Peng, B.; Zhao, D.; Wong, T. K. S.; Xiong, Q.; Wei, X.; Heeger, A. J., A Plasmonically Enhanced Polymer Solar Cell with Gold – Silica Core – Shell Nanorods. *Org. Electron.* **2013**, *14*, 2360-2368.
26. Gao, Y.; MacKenzie, R. C. I.; Liu, Y.; Xu, B.; Loosdrecht, P. H. M. v.; Tian, W., Engineering Ultra Long Charge Carrier Lifetimes in Organic Electronic Devices at Room Temperature. *Adv. Mater. Interfaces* **2015**, *2*, 1400555.
27. MacKenzie, R. C. I.; Shuttle, C. G.; Dibb, G. F.; Treat, N.; Hauff, E. v.; Robb, M. J.; Hawker, C. J.; Chabynyc, M. L.; Nelson, J., Interpreting the Density of States Extracted from Generic Solar Cells Using Transient Photocurrent Measurements. *J. Phys. Chem. C* **2013**, *117*, 12407-12414.

28. Aouani, H.; Rahmani, M.; Navarro-Cía, M.; Maier, S. A., Third-Harmonic-Upconversion Enhancement from a Single Semiconductor Nanoparticle Coupled to a Plasmonic Antenna. *Nature Nanotech.* **2014**, *9*, 290-294.
29. Rodal-Cedeira, S., et al., Plasmonic Au@Pd Nanorods with Boosted Refractive Index Susceptibility and Sens Efficiency: A Multifunctional Platform for Hydrogen Sensing and Monitoring of Catalytic Reactions. *Chem. Mater.* **2016**, *28*, 9169-9180.
30. Knight, M. W.; Wang, Y.; Urban, A. S.; Sobhani, A.; Zheng, B. Y.; Nordlander, P.; Halas, N. J., Embedding Plasmonic Nanostructure Diodes Enhances Hot Electron Emission. *Nano Lett.* **2013**, *13*, 1687-1692.
31. Kojori, H. S.; Yun, J.-H.; Paik, Y.; Kim, J.; Anderson, W. A.; Kim, S. J., Plasmon Field Effect Transistor for Plasmon to Electric Conversion and Amplification. *Nano Lett.* **2016**, *16*, 250-254.
32. Webb, J. A.; Aufrecht, J.; Hungerford, C.; Bardhan, R., Ultrasensitive Analyte Detection with Plasmonic Paper Dipsticks and Swabs Integrated with Branched Nanoantennas. *J. Materials Chemistry C* **2014**, *2*, 10446 - 10454.
33. Lu, L.; Luo, Z.; Xu, T.; Yu, L., Cooperative Plasmonic Effect of Ag and Au Nanoparticles on Enhancing Performance of Polymer Solar Cells. *Nano Letters* **2013**, *13*, 59-64.
34. Menke, S. M.; Holmes, R. J., Exciton Diffusion in Organic Photovoltaic Cells. *Energ. Environ. Sci.* **2014**, *7*, 499-512.
35. Molitin, A.; Nunzi, J.-M., How to Model the Behaviour of Organic Photovoltaic Cells. *Polym. Int.* **2006**, *55*, 583-600.
36. Armin, A.; Juska, G.; Ullah, M.; Velusamy, M.; Burn, P. L.; Meredith, P.; Pivrikas, A., Balanced Carrier Mobilities: Not a Necessary Condition for High-Efficiency Thin Organic Solar Cells as Determined by Mis-Celiv. *Adv. Energ. Mater.* **2014**, *4*, 1-8.
37. Johnson, P. B.; Christy, R. W., Optical Constants of the Noble Metals. *Phys. Rev. B* **1972**, *6*, 4370-4379.
38. Mackenzie, R. C. I.; Kirchartz, T.; Dibb, G. F. A.; Nelson, J., Modeling Nongeminate Recombination in P3ht : Pcbm Solar Cells. *J. Phys. Chem. C* **2011**, *115*, 9806-9813.
39. Mackenzie, R. C. I.; Shuttle, C. G.; Chabinye, M. L.; Nelson, J., Extracting Microscopic Device Parameters from Transient Photocurrent Measurements of P3ht : Pcbm Solar Cells Communication. *Adv. Energ. Mater.* **2012**, *2*, 662-669.
40. Clarke, T.; Ballantyne, A.; Jamieson, F.; Brabec, C.; Nelson, J.; Durrant, J., Transient Absorption Spectroscopy of Charge Photogeneration Yields and Lifetimes in a Low Bandgap Polymer/Fullerene Film. *Chem. Comm.* **2009**, 7345, 89-91.
41. Namkoong, G.; Boland, P.; Lee, K.; Dean, J.; Namkoong, G.; Boland, P.; Lee, K.; Dean, J., Design of Organic Tandem Solar Cells Using Pcpdtbt : Pc 61 Bm and P3ht : Pc 71 Bm. *J. Appl. Phys.* **2010**, *107*, 124515-124515.
42. Etzold, F.; Howard, I.; Mauer, R.; Meister, M.; Kim, T. D.; Lee, K. S.; Baek, N. S.; Laquai, F., Ultrafast Exciton Dissociation Followed by Nongeminate Charge Recombination in Pcdtbt:Pcbm Photovoltaic Blends. *J. Am. Chem. Soc* **2011**, *133*, 9469-79.
43. Proctor, C. M.; Kuik, M.; Nguyen, T.-Q., Charge Carrier Recombination in Organic Solar Cells. *Prog. Polym. Sci.* **2013**, *38*, 1941-1960.
44. Choi, H.; Lee, J.-P.; Ko, S.-J.; Jung, J.-W.; Park, H.; Yoo, S.; Park, O.; Jeong, J.-R.; Park, S.; Kim, J. Y., Multipositional Silica-Coated Silver Nanoparticles for High-Performance Polymer Solar Cells. *Nano Lett.* **2013**, *13*, 2204-8.

45. Wu, B.; Wu, X.; Guan, C.; Fai Tai, K.; Yeow, E. K. L.; Jin Fan, H.; Mathews, N.; Sum, T. C., Uncovering Loss Mechanisms in Silver Nanoparticle-Blended Plasmonic Organic Solar Cells. *Nat. Commun.* **2013**, *4*, 1-7.
46. Erwin, W. R.; Zarick, H. F.; Talbert, E. M.; Bardhan, R., Light Trapping in Mesoporous Solar Cells with Plasmonic Nanostructures. *Energy Environ. Sci.* **2016**, *9*, 1577-1601.
47. Zarick, H. F.; Boulesba, A.; Puretzky, A. A.; Talbert, E. M.; Debra, Z.; Soetan, N.; Geohegan, D. B.; Bardhan, R., Ultrafast Carrier Dynamics in Bimetallic Nanostructures-Enhanced Methylammonium Lead Bromide Perovskites. *Nanoscale* **2017**, *9*, 1475-1483
48. Zarick, H. F.; Erwin, W. R.; Boulesbaa, A.; Hurd, O.; Webb, J. A.; Puretzky, A.; Geohegan, D.; Bardhan, R., Improving Light Harvesting in Dye Sensitized Solar Cells Using Hybrid Bimetallic Nanostructures. *ACS Photonics* **2016**, *3*, 385-394.
49. Zhou, L.; Tan, Y.; Wang, J.; Xu, W.; Yuan, Y.; Cai, W.; Zhu, S.; Zhu, J., 3d Self-Assembly of Aluminium Nanoparticles for Plasmon-Enhanced Solar Desalination. *Nature Photonics* **2016**, *10*, 393-398.
50. Neumann, O.; Urban, A. S.; Day, J.; Lal, S.; Nordlander, P.; Halas, N. J., Solar Vapor Generation Enabled by Nanoparticles. *ACS Nano* **2013**, *7*, 42-49.
51. Webb, J. A.; Erwin, W. R.; Zarick, H. F.; Aufrecht, J.; Manning, H.; Lang, M. J.; Pint, C. L.; Bardhan, R., Geometry Dependent Plasmonic Tunability and Photothermal Characteristics of Multibranch Gold Nanoantennas. *J. Physical Chemistry C* **2014**, *118*, 3696-3707.
52. Battaglia, C., et al., Light Trapping in Solar Cells : Can Periodic Beat Random? *ACS Nano* **2012**, *6*, 2790-2797.
53. Ferry, V. E.; Verschuuren, M. A.; Li, H. B. T.; Verhagen, E.; Walters, R. J.; Schropp, R. E. I.; Atwater, H. A.; Polman, A., Light Trapping in Ultrathin Plasmonic Solar Cells. *Opt. Express* **2010**, *18*, A237-45.